

Unified Definition of Exciton Coherence Length for Exciton–Phonon Coupled Molecular Aggregates

Tong Jiang, Jiajun Ren, and Zhigang Shuai*



Cite This: *J. Phys. Chem. Lett.* 2023, 14, 4541–4547



Read Online

ACCESS |



Metrics & More

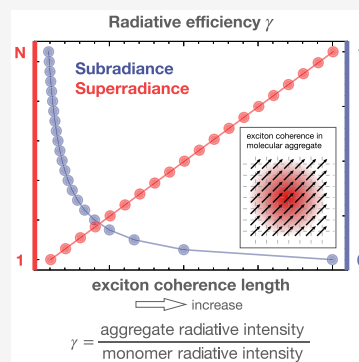


Article Recommendations



Supporting Information

ABSTRACT: Exciton coherence length (ECL) characterizes the spatial extent of coherently delocalized excited states of molecular aggregates. Constructive/destructive superpositions of coherent molecular dipoles lead to superradiance/subradiance, where the radiative rate is enhanced/suppressed compared to that of a single molecule. Longer ECLs correspond to faster/slower radiative rates for superradiant/subradiant aggregates. However, previous ECL definitions fail to produce monotonic relationships when exciton–phonon coupling is considered, even for simple 1D exciton–phonon systems. This problem is exacerbated for 2D aggregates with both constructive and destructive superpositions. In this Letter, we propose a novel ECL definition by virtue of sum rule for oscillator strengths, ensuring a bijective and monotonic relationship between ECL and radiative rate for both 1D/2D superradiant and subradiant aggregates. Using numerically accurate time-dependent matrix product states, we study large-scale, exciton–phonon coupled 2D aggregates and predict the existence of maximum superradiance at finite temperature, in contrast to the previously believed $1/T$ law. Our results provide new insights into the design and optimization of efficient light emitting materials.



Molecular aggregates have received widespread interest due to their promising applications in diverse fields, such as biological photosynthesis,^{1,2} organic light-emitting materials, lasers, energy conversion technologies (e.g., photovoltaics and thermoelectrics), and field effect transistors.^{3–6} Great progress in experiments and theories have deepened the understanding of the excited states of molecular aggregates—excitons.⁷ Excitons in molecular aggregates are collective excitations comprising superpositions of local excitations, where molecules subject to photoabsorption exchange excitation energy through transition dipole–dipole interactions, also known as excitonic coupling.⁸ Kasha’s theory models molecular aggregates as linear chains and clarifies them as J aggregate (with negative excitonic coupling) and H aggregate (with positive excitonic coupling). In J aggregate, the local dipole oscillation constructively adds up, resulting in superradiance enhancement,^{9–13} which refers to the increased oscillator strength and thus the radiative rate compared to that of a single molecule. In contrast, the destructive phase between the dipoles in H aggregate leads to quenched fluorescence, known as subradiance.^{13–16} The ideal exciton is fully coherent over the entire domain for aggregates composed of N disorder-free rigid molecules at zero temperature, leading to N times enhancement of the fluorescence rate for J aggregate and complete quenching for H aggregate. In reality, due to the soft nature, organic π -conjugated molecules undergo substantial structure reorganizations upon excitation and the exciton is spatially localized to a subset of the aggregate in subpicoseconds or picoseconds due to the coupling to high-frequency modes^{13,17} or low-frequency modes.^{18,19} The exciton coher-

ence length (ECL) measures the spatial distance over which the exciton is delocalized, and there are other localization mechanisms including static disorder and temperature.^{20,21} The ECL dictates the optical response in molecular aggregates such as superradiance and exciton transport. Chemical systems such as biological systems, optoelectric functional devices have been incorporating molecular aggregates with long ECL and thus enhanced optical responses^{21–25} to enhance function. Therefore, gaining a better understanding of how aggregate properties influence the ECL is of paramount importance. For 1D system, increasing the excitonic coupling leads to larger ECL, resulting in stronger enhancement/suppression of the radiative rate for molecular aggregate with negative/positive couplings. This effect can be tuned by changing the packing angles, distances between molecules, or number of interacting molecules.^{8,16,21} A defining feature of 2D molecular aggregate is the coexistence of positive and negative couplings,^{26–30} making it unclear in how the ECL of 2D system changes with temperature, packing structure, etc.

Unfortunately, ECL has long been poorly defined even for 1D exciton–phonon coupled aggregates. One method to calculate ECL is through the calculation of the emission

Received: March 27, 2023

Accepted: May 5, 2023

intensity ratio between 0–0 and 0–1 peak,³¹ which is limited to J aggregates consisting of molecules coupled to a high-frequency intramolecular mode. The exciton reduced density matrix, which is obtained by tracing the phonon degrees of freedom of the total density matrix,^{32,33} is the most relevant physical quantity to exciton coherence. The reduced density matrix depicts the system at thermal equilibrium and serves as the initial state for quantum dynamics simulations of open quantum systems.³⁴ When the exciton population thermalizes rapidly on the time scale of exciton lifetime, the Boltzmann distribution is maintained throughout the radiative process,^{10,35} thereby dictating the radiative decay rate. The exciton coherence length, which is correlated with the radiative rate, can therefore be extracted from the reduced density matrix. Multiple definitions of ECL have been proposed to understand the coherence and its relation to radiative efficiency.^{20,36–38} However, their generalization to complex cases is questioned as different definitions of ECL lead to even qualitative differences for the temperature dependence of coherence.³⁴ Therefore, the use of these definitions should be cautioned. The purpose of this Letter is to give a unified definition of ECL that connects rigorously with the radiative rate in complex molecular aggregates. Such a definition will guide the rational design of high-performance 2D molecular aggregates with properties such as superradiance or efficient exciton transport.

The importance of exciton reduced density matrix cannot be overstated, yet only a few numerically exact methods have been employed for its calculation. We recently developed an algorithm that combined the imaginary time evolution^{39,40} with the matrix product states (MPS) to accurately calculate the thermal equilibrium density matrix of the high dimensional exciton–phonon systems across a broad range of parameter regimes.⁴¹ The optimal matrix product operator (MPO) factorization of general exciton–phonon Hamiltonians is automatically generated with a graph theory based algorithm.⁴² Theoretical studies of the photophysics of molecular aggregates generally rely on the celebrated Frenkel–Holstein model:⁴³

$$\hat{H} = \sum_{m,n} J_{mn} a_m^\dagger a_n + \sum_n \sum_i^{N_{\text{ph}}} \omega_{ni} b_{ni}^\dagger b_{ni} + \sum_n \sum_i^{N_{\text{ph}}} \omega_{ni} g_{ni} a_n^\dagger a_n (b_{ni}^\dagger + b_{ni}) \quad (1)$$

where N molecules are coupled to a set of N_{ph} phonon modes with frequency ω_{ni} and coupling strength g_{ni} . $S_{ni} = g_{ni}^2$ is also known as the Huang–Rhys factor. The excitonic coupling J_{mn} describes the transition dipole–dipole interaction between molecules ($m \neq n$). a_n^\dagger (a_n) is the raising (lowering) operator for local excitation, and b_{ni}^\dagger (b_{ni}) is the phononic creation (annihilation) operator associated with the i th phonon mode coupled to the n th molecule. While the charge transfer state is not considered here, it could also be a contributing factor to the emission properties, as discovered recently.^{44–48} We want to comment that if charge transfer state is involved, the intermolecular phonon mode could also be important.^{47,48} Here, we only consider intramolecular phonon. The thermal equilibrium density matrix ρ_β of a mixed state in physical space P can be obtained by performing the partial trace of the pure state in the double space $P \otimes Q$,

$$\hat{\rho}_\beta = \frac{e^{-\beta\hat{H}}}{Z} = \frac{\text{Tr}_Q |\psi_\beta\rangle\langle\psi_\beta|}{\text{Tr}_Q |\psi_\beta\rangle\langle\psi_\beta|}, \quad |\psi_\beta\rangle = e^{-\beta\hat{H}/2} \sum_i |i\rangle_P |i\rangle_Q \quad (2)$$

where $\beta = 1/k_B T$. The many-body wave function $|\psi_\beta\rangle$ in the enlarged space is approximated as MPS, as shown in Figure 1.

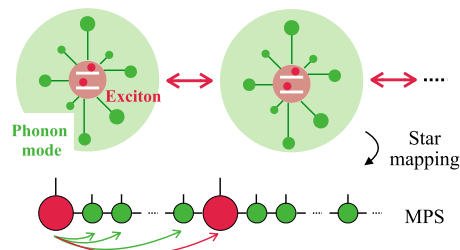


Figure 1. Scheme illustrating the mapping of the interacting excitons coupled with phonons yielding the MPS representation in the simulations.

It is obtained by the propagation of the maximally entangled state along the imaginary time axis to $-\beta/2$ employing the time dependent variational principle with projector splitting algorithm.⁴⁹

The radiative efficiency of the N site molecular aggregate is defined as the ratio between its oscillator strength over that of an isolated molecule,

$$\gamma = \frac{\int d\omega I_N^\alpha(\omega)}{\int d\omega I_1^\alpha(\omega)} \quad (3)$$

$$I_N^\alpha(\omega) = \sum_{uv} \frac{e^{-\beta E_v}}{Z} |\langle \hat{\mu}_\alpha | \hat{u}_\alpha | \phi_u \rangle|^2 \delta(\omega - E_{uv}) \quad (4)$$

where $I_N^\alpha(\omega)$ is the expression of the dimensionless steady-state α -polarized fluorescence spectrum ($\alpha \in (x, y, z)$) for N -site molecular aggregates. The transition dipole operator $\hat{\mu} = \mu_\alpha \sum_i^N (a_i^\dagger + a_i)$, $E_{uv} = E_u - E_v$, $|\phi_u\rangle$ and $|\phi_v\rangle$ are eigenstates of the whole system including excitons and phonons, and they are in the set of ground states and excited states separately. The integration of $I(\omega)$ over frequency is equal to the oscillator strength. A certified ECL bridges the radiative efficiency γ and coherence of molecular aggregates. Different ECLs have been defined as a function of the reduced density matrix:^{20,34,36–38}

$$L_1 = \frac{(\sum_{mn} |\rho_{mn}|)^2}{N \sum_{mn} |\rho_{mn}|^2}, \quad 1 \leq L_1 \leq N \quad (5)$$

$$L_2 = \sum_{m \geq n} |\rho_{mn}|, \quad 1 \leq L_2 \leq \frac{N+1}{2} \quad (6)$$

$$L_3 = N \text{Tr} \rho^2, \quad 1 \leq L_3 \leq N \quad (7)$$

where L_1 corresponds to the variance of the reduced density matrix, L_2 sums the absolute values of the upper triangles of the reduced density matrix, and L_3 makes use of the purity of density matrix ($\text{Tr} \rho^2 \leq 1$, the equivalence holds for pure state). All these definitions give a monotonic and bijective relationship between the ECL and radiative efficiency in the case of purely excitonic systems (Figure S2), i.e., without considering the interplay of phonons. After taking the exciton–

phonon couplings into consideration, we calculate the reduced density matrix ρ by tracing the phonon degrees of freedom of the total Boltzmann operator obtained by time dependent matrix product states for eq 2:

$$\rho = \text{Tr}_{\text{ph}} \hat{\rho}_{\beta} \quad (8)$$

with elements $\rho_{mn} = \text{Tr}(a_m^{\dagger} a_n \hat{\rho}_{\beta})$ containing the coherence between molecule m and n . Note that there are also experimental protocols to measure the reduced density matrix by quantum tomography via ultrafast spectroscopy.³³

We select the 2D brick-layer molecular aggregate as the research object, as illustrated in Figure 2(a), and the reasons

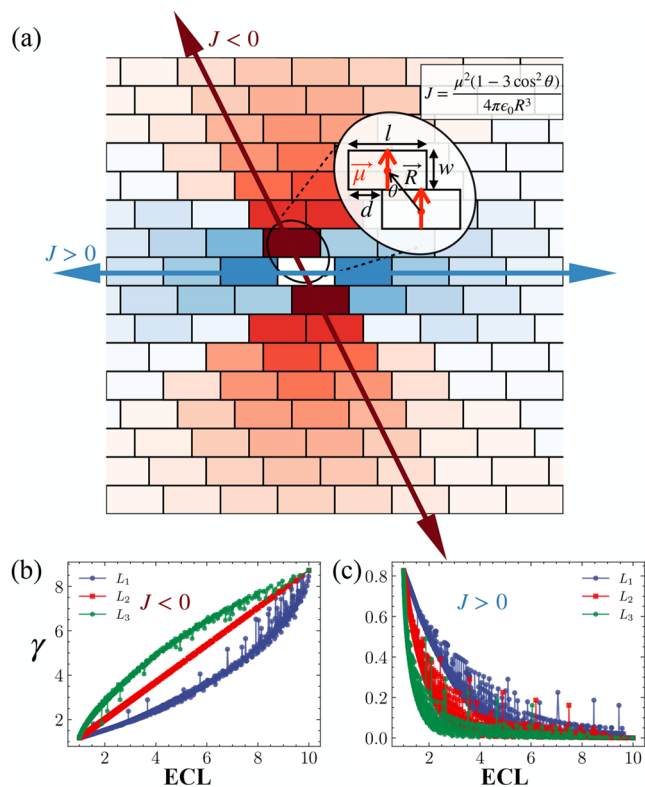


Figure 2. (a) Illustration of the 2D brick-layer where red/blue colors represent negative/positive excitonic couplings with the centered molecule (in white). The relationship between γ and ECL for 1D selected axis in the 2D setup for (b) $J < 0$ (c) $J > 0$.

are 2-fold. First, many organic semiconductors based on dyes/color pigments are packed with the 2D brick-layers including the first experimentally discovered J aggregate.^{50,51} Its importance was recognized for bringing efficient fluorescence, exciton transport, and hole/electron transport in two dimensions.²³ Second, technically such a setup possesses an exciton coupling structure that is complicated enough with the coexistence of positive and negative long-range excitonic couplings,²⁹ which serves as a very good touchstone to examine the feasibility of ECLs. We model 2D aggregates packed with slipped brick-layers with inhomogeneous excitonic couplings which change strengths and signs for different pairs of molecules). The slips between molecules can be experimentally tuned by making use of steric hindrances or hydrogen bonds.^{22,27} We change the geometry by adjusting the slip distance between layers to get different excitonic coupling patterns. The couplings are distinguished by red for negative

coupling and blue for positive coupling, and the color depth indicates the strength of couplings. As indicated in Figure 2(a), the excitonic coupling between two bricks $J = \mu^2(1 - 3 \cos^2 \theta) / 4\pi\epsilon_0 R^3$, where \vec{R} is the displacement vector between bricks, θ is the angle between \vec{R} and the transition dipole vector $\vec{\mu}$, and ϵ_0 is the dielectric constant in the medium.

We first extract two 10-site 1D systems from two axes of the 2D brickwork, corresponding to the case of $J > 0$ (H aggregate) and $J < 0$ (J aggregate) separately, as shown in Figure 2(b)(c). The benchmarks are shown in Figure S3. Each molecule couples to two phonon modes: a high-frequency mode with frequency ω and Huang–Rhys factor $S_1 \in [0, 0.5]$, that represents the ubiquitous vinyl stretching/ring breathing vibration observed in most conjugated molecules, and a low-frequency mode with frequency 0.1ω that corresponds to such as torsional motions. Lots of studies employed only a high-frequency phonon mode for modeling the quantum dynamics and spectroscopy of molecular aggregates and explaining experimental results.¹³ The low-frequency mode also reflects the effect of static disorder since the phonon moves quite slowly compared with the exciton when $J \gg \omega$,⁵² leading to a modification of onsite excitation energy that barely changes in the time scale of exciton motion, as proven analytically⁵³ and numerically in Figure S1. Our setup considers excitonic coupling, high and low frequency intramolecular phonons, and temperature, which is enough to cover a wide range of coupling regimes to examine the ECLs. We plot the relationship between ECL with different definitions and γ in Figure 2. Among the parameters studied in Figure 2, the excitonic coupling for nearest neighbor coupling is adjusted from 0.1ω to ω (the absolute values of long-range couplings are also considered which decrease with $1/|R_{ij}|^3$ where $|R_{ij}|$ is the distance between molecules, and the Huang–Rhys factor of the low frequency mode changes from 0 to 5.0, and the temperature ranges from 0 to 2.0ω). The chosen parameters ensure a broad parameter regime that covers from the localization limit to the delocalization limit. The absolute values of ECLs are all scaled to let $1 \leq L \leq N$ for comparison (see eqs 5–7), since we are particularly interested in the ability of ECLs of reflecting the changes of γ . As shown in Figure 2(b)(c), nonmonotonous and nonbijective correlations between the radiative efficiency and ECLs are observed, in contrast to the purely excitonic case presenting monotonic and bijective relations (Figure S2). It should be noted that L_2 correlates monotonically with γ only in superradiant systems, and not in subradiant systems. In subradiant 1D systems, a larger ECL should lead to smaller radiative decay rate.⁴⁴ We also note the inappropriate faster growing ECL of L_1 near the limit of complete delocalization, which results in the case that systems have similar ECLs but vastly different radiative efficiency (Figure S4).

Because of the failure of the available ECLs for 1D systems, they are generally not suitable to be used in the common real-world 2D systems, one defining feature of which is the coexistence of positive and negative couplings, as exemplified in Figure 2(a). In Figure 3, we change the coupling strength by adjusting the nearest-neighbor coupling J_0 for $d = 0$ along the vertical axis, i.e., $J_0 = \frac{\mu^2}{2\pi\epsilon_0 w^3}$ where w is the brick width (other pairs of couplings are calculated with $J = \mu^2(1 - 3 \cos^2 \theta) / 4\pi\epsilon_0 R^3$). By varying the slip distance d , we observe the change of γ with ECLs, as shown in Figure 3. In the weak coupling

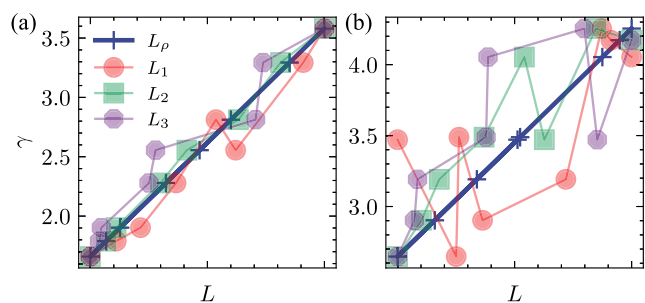


Figure 3. (a) $J_0 = \omega$ and (b) $J_0 = 2\omega$ for 10×10 bricks with open boundary condition. J_0 is the nearest-neighbor coupling along the vertical axis for $d = 0$, i.e., the coupling strength for two face-to-face packed molecules without slips. The phonon mode is with frequency ω and $g = 1$. $M = 64$ is used. ECLs with different definitions have been scaled for comparison.

case, the ECLs agree well with γ as the slip distance changes. However, for large couplings, previously defined ECLs display

qualitative differences. This problem appears even in the case that the exciton–phonon couplings are not taken into account, see Figure S6.

Against the fact that previously proposed ECLs cannot correlate well with radiative efficiency, we propose the following definition:

$$L_\rho = \left(\sum_{mn} \rho_{mn} + \frac{1}{N} \right)^{\Theta(\sum_{mn} \rho_{mn} - 1)} \quad (9)$$

where $\Theta(x)$ is a step function that is -1 for $x \leq 0$ and 1 for $x > 0$. This function builds monotonic and bijective correlation between ECL and radiative efficiency for superradiant or subradiant aggregates (see Figure S5) since it utilizes the fact that the summation of all elements of the reduced density matrix is equal to the radiative efficiency γ . It is straightforward to check the equivalence between γ and $\sum_{mn} \rho_{mn}$, which is a kind of sum rule $\int d\omega I_N(\omega) = \text{Tr}(\hat{\rho}_\beta \hat{\mu} \hat{\mu})$. The computational

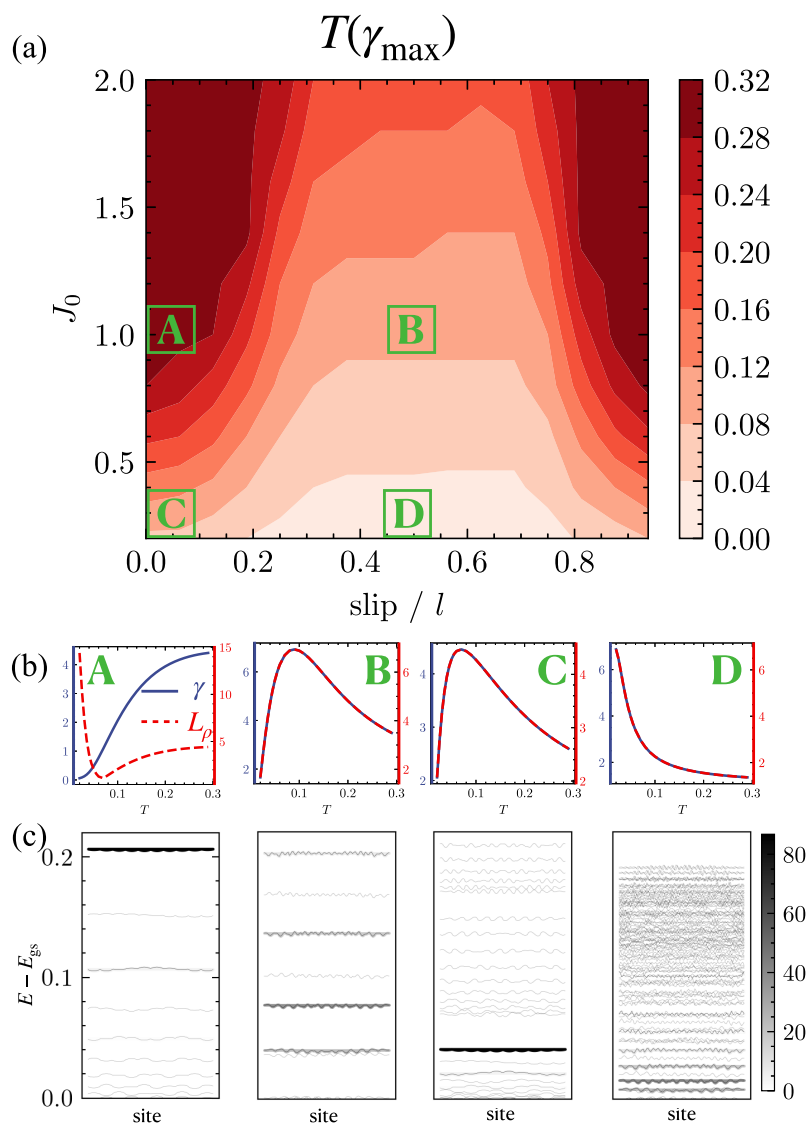


Figure 4. (a) The temperature for maximum superradiance for different slip distances and couplings. (b) Four exemplary cases that illustrate the temperature dependence of γ and L_ρ and (c) the corresponding wavefunctions with combining coefficients for the local sites, whose color depth indicates the oscillator strength of that energy level.

time can also be greatly saved since it is unnecessary to perform a dynamical response calculation with expensive real time evolutions (eq 4) to calculate γ , which enables the efficient simulation of large-scale systems. It is useful to analyze the limiting cases. In the complete coherence limit of superradiant ($\gamma > 1$) and subradiant ($\gamma < 1$) molecular aggregates, the reduced density matrix is ideally formulated as

$$\rho_{mn} = 1/N, L_p = N + 1/N \sim N \quad \text{superradiant} \quad (10)$$

$$\rho_{mn} = (-1)^{m-n}/N, L_p = N \quad \text{subradiant} \quad (11)$$

In the complete localization limit for both superradiant and subradiant aggregates

$$\rho_{mn} = \delta_{mn}/N, L_p = N/(N + 1) \sim 1 \quad (12)$$

Starting from the reduced density matrix, a determined value of ECL is connected with the γ , which is different from previous definitions that have nonbijective connections. Such a definition also ensures a linear relationship for the superradiant case and is also related to the concept of quantum Fisher information that measures the multipartite entanglement in quantum metrology of an exciton system.⁵⁴ As shown in Figure 3, L_p correlates linearly with the radiative efficiency γ in the 2D exciton–phonon coupled molecular aggregate.

The new definition of ECL bridges the bijective relationship with the superradiance enhancement (SRE) of the 2D aggregate, which is defined as the *enhanced* ratio of the oscillator strength of the molecular aggregate over that of an isolated molecule ($\gamma > 1$ in eq 3). We can efficiently obtain the SRE of a large-scale 2D aggregate (10×10). This allows us to look into the function–structure relationship of 2D aggregates including but not limited to the brick-layer setup we used here. We study the temperature dependence of SRE. The temperature dependence of SRE in 2D *isotropic* systems is well-described by the $1/T$ law.⁵⁵ This behavior has also been observed experimentally in brick-layer structured 2D systems with *anisotropic* intermolecular coupling.²⁶ Specifically, the maximal SRE is achieved at zero temperature, and SRE decreases as the temperature is increased.

Here, we predict a new temperature dependence of the SRE for a slipped 2D molecular aggregate, as shown in Figure 4. We observe an unusual nonmonotonous temperature dependence of SRE in the 2D aggregates, and maximal SRE at a finite temperature ($T(\gamma_{\max}) > 0$) is possible, in contrary to the previous $1/T$ behavior. We plot the temperature when achieving maximal SRE for different excitonic couplings and slips in Figure 4(a). The temperature dependence experiences a transition when temperature increases to a certain point $T(\gamma_{\max})$, after which the SRE decreases with increasing temperature. It is shown that $T(\gamma_{\max})$ becomes larger for larger excitonic coupling. We select 4 exemplary cases (A, B, C, D) in Figure 4(a)(b) with different temperature dependences for γ and L_p . The coupling patterns are shown in Figure S7. For case A, the SRE keeps increasing with the increase of temperature, which is totally different from a traditional J aggregate whose SRE decreases as temperature increases. In a traditional J aggregate, most of the oscillator strengths are located in the lowest excited state, and the increased temperature reduces the thermal population on the lowest state, leading to decreased SRE. In a traditional H aggregate, the oscillator strengths are located in the highest excited states, thus the increased temperature increases the population on the highest states, leading to increased radiative efficiency but will

not exceed 1. Case A totally violates the temperature dependence of the radiative efficiency of traditional J and H aggregates: it is superradiant as a J aggregate, but the radiative efficiency grows with increasing temperature, just like an H aggregate. Such temperature-activated superradiance has also been observed in polymer model systems composed of two chains.^{13,30} In these systems, the radiative decay rate starts out as subradiant due to the H-like interactions between chains, but eventually becomes superradiant due to the J-like interactions within chains. Case D behaves as a traditional J aggregate. By contrast, the SRE of cases B and C first increases with temperature and then decreases.

We explain this by directly diagonalizing the exciton Hamiltonian and get the wavefunction amplitudes of each site and the oscillator strength of each energy level in Figure 4(c). We note that the fast phonon does not qualitatively change the temperature dependence of the SRE, as shown in Figure S8. The energy of the ground state energy is set as the zero point. For case A, the energy levels with energy below 0.2 carry very little oscillator strength, while the oscillator strength concentrates on the high energy level; therefore, γ keeps increasing with increasing temperature since the occupation of the bright state becomes larger. At the very low temperature of case A, the exciton is distributed mainly at the low energy levels which is very delocalized but with destructive wavefunction amplitudes. It is observed that the radiative efficiency is lower than 1, which is the characteristic of an H aggregate. As temperature increases, the occupation of the lowest levels becomes smaller, and the coherence decreases until γ grows to 1 which marks the transition to the J aggregate. The occupation of the high coherent level with large oscillator strengths becomes larger, and the SRE increases with temperature. Contrary to case A, the SRE and ECL of case D decreases with increasing temperature since the coherent bright state is located at the bottom. The coherent bright states of case B and C are located in the middle of the energy diagrams; therefore, the SRE experiences a thermal activation at low temperature, after which it decreases with increasing temperature.

In summary, our study provided a unified definition of exciton coherence length (ECL) for exciton–phonon coupled molecular aggregates. Previous definitions based on variance, off-diagonal elements, or the purity of reduced density matrix cannot correlate ECL with the radiative efficiency monotonically for superradiant and subradiant aggregates, and can lead to qualitative differences. Our new definition is derived by virtue of sum rule of oscillator strength, and guarantees a monotonic and bijective connection between the ECL and radiative efficiency for 1D/2D superradiant and subradiant aggregates. The unified ECL serves as an efficient and reliable quantity to measure coherence related optical properties such as superradiance in complex systems. We use the numerically accurate time-dependent matrix product states to investigate two-dimensional molecular aggregates and rigorously demonstrate that our ECL connects with the superradiance enhancement. Our results suggested a new temperature dependence of superradiance and coherence in 2D aggregates with brick-wall packing structures. We note that while we can consider both high and low frequency phonon modes (see Supporting Information), we acknowledge that our model is an idealized representation of the real-world systems since realistic molecular aggregates may have more complex exciton–phonon

couplings. Our study provides new insights that can be used in the design of light emitting materials.

■ ASSOCIATED CONTENT

SI Supporting Information

The Supporting Information is available free of charge at <https://pubs.acs.org/doi/10.1021/acs.jpcllett.3c00812>.

Benchmarks, ECL in pure exciton systems, slow phonon mimics the effect of static disorder, etc. (PDF)
Transparent Peer Review report available (PDF)

■ AUTHOR INFORMATION

Corresponding Author

Zhigang Shuai – MOE Key Laboratory of Organic Optoelectronics and Molecular Engineering, Department of Chemistry, Tsinghua University, Beijing 100084, People's Republic of China; School of Science and Engineering, The Chinese University of Hong Kong, Shenzhen, Guangdong 518172, People's Republic of China; orcid.org/0000-0003-3867-2331; Email: zgsuai@tsinghua.edu.cn

Authors

Tong Jiang – MOE Key Laboratory of Organic Optoelectronics and Molecular Engineering, Department of Chemistry, Tsinghua University, Beijing 100084, People's Republic of China; orcid.org/0000-0002-5907-4886

Jiajun Ren – MOE Key Laboratory of Theoretical and Computational Photochemistry, College of Chemistry, Beijing Normal University, Beijing 100875, People's Republic of China; orcid.org/0000-0002-1508-4943

Complete contact information is available at:

<https://pubs.acs.org/doi/10.1021/acs.jpcllett.3c00812>

Notes

The authors declare no competing financial interest.

■ ACKNOWLEDGMENTS

This work is supported by the National Natural Science Foundation of China (NSFC) through the project "Science Center for Luminescence from Molecular Aggregates (SCELMA)" Grant Number 21788102, as well as by the Ministry of Science and Technology of China through the National Key R&D Plan Grant Number 2017YFA0204501.

■ REFERENCES

- (1) Cao, J.; Cogdell, R. J.; Coker, D. F.; Duan, H.-G.; Hauer, J.; Kleinekathöfer, U.; Jansen, T. L.; Mančal, T.; Miller, R. D.; Ogilvie, J. P.; et al. Quantum biology revisited. *Sci. Adv.* **2020**, *6*, No. eaaz4888.
- (2) Jang, S. J.; Mennucci, B. Delocalized excitons in natural light-harvesting complexes. *Rev. Mod. Phys.* **2018**, *90*, 035003.
- (3) Wei, Y.-C.; Wang, S. F.; Hu, Y.; Liao, L.-S.; Chen, D.-G.; Chang, K.-H.; Wang, C.-W.; Liu, S.-H.; Chan, W.-H.; Liao, J.-L.; et al. Overcoming the energy gap law in near-infrared OLEDs by exciton-vibration decoupling. *Nat. Photonics* **2020**, *14*, 570–577.
- (4) Jin, X.-H.; Price, M. B.; Finnegan, J. R.; Boott, C. E.; Richter, J. M.; Rao, A.; Menke, S. M.; Friend, R. H.; Whittell, G. R.; Manners, I. Long-range exciton transport in conjugated polymer nanofibers prepared by seeded growth. *Science* **2018**, *360*, 897–900.
- (5) Liu, R.; Ge, Y.; Wang, D.; Shuai, Z. Understanding the Temperature Dependence of the Seebeck Coefficient from First-Principles Band Structure Calculations for Organic Thermoelectric Materials. *CCS Chem.* **2021**, *3*, 1477–1483.
- (6) Ostroverkhova, O. Organic optoelectronic materials: mechanisms and applications. *Chem. Rev.* **2016**, *116*, 13279–13412.
- (7) Dimitriev, O. P. Dynamics of Excitons in Conjugated Molecules and Organic Semiconductor Systems. *Chem. Rev.* **2022**, *122*, 8487–8593.
- (8) Zhang, Y.; Luo, Y.; Zhang, Y.; Yu, Y.-J.; Kuang, Y.-M.; Zhang, L.; Meng, Q.-S.; Luo, Y.; Yang, J.-L.; Dong, Z.-C.; et al. Visualizing coherent intermolecular dipole–dipole coupling in real space. *Nature* **2016**, *531*, 623–627.
- (9) Gross, M.; Haroche, S. Superradiance: An essay on the theory of collective spontaneous emission. *Phys. Rep.* **1982**, *93*, 301–396.
- (10) Spano, F. C.; Kuklinski, J. R.; Mukamel, S. Temperature-dependent superradiant decay of excitons in small aggregates. *Phys. Rev. Lett.* **1990**, *65*, 211.
- (11) Heijs, D.; Malyshev, V.; Knoester, J. Decoherence of excitons in multichromophore systems: thermal line broadening and destruction of superradiant emission. *Phys. Rev. Lett.* **2005**, *95*, 177402.
- (12) Eisfeld, A.; Marquardt, C.; Paulheim, A.; Sokolowski, M. Superradiance from two dimensional brick-wall aggregates of dye molecules: the role of size and shape for the temperature dependence. *Phys. Rev. Lett.* **2017**, *119*, 097402.
- (13) Hestand, N. J.; Spano, F. C. Expanded theory of H- and J-molecular aggregates: the effects of vibronic coupling and intermolecular charge transfer. *Chem. Rev.* **2018**, *118*, 7069–7163.
- (14) Kasha, M. Energy transfer mechanisms and the molecular exciton model for molecular aggregates. *Radiat. Res.* **1963**, *20*, 55–70.
- (15) Kasha, M.; Rawls, H. R.; El-Bayoumi, M. A. The exciton model in molecular spectroscopy. *Pure Appl. Chem.* **1965**, *11*, 371–392.
- (16) Trebbia, J.-B.; Deplano, Q.; Tamarat, P.; Lounis, B. Tailoring the superradiant and subradiant nature of two coherently coupled quantum emitters. *Nat. Commun.* **2022**, *13*, 1–9.
- (17) Park, K. H.; Kim, W.; Yang, J.; Kim, D. Excited-state structural relaxation and exciton delocalization dynamics in linear and cyclic π -conjugated oligothiophenes. *Chem. Soc. Rev.* **2018**, *47*, 4279–4294.
- (18) Binder, R.; Lauvergnat, D.; Burghardt, I. Conformational dynamics guides coherent exciton migration in conjugated polymer materials: First-principles quantum dynamical study. *Phys. Rev. Lett.* **2018**, *120*, 227401.
- (19) Deutsch, M.; Wirsing, S.; Kaiser, D.; Fink, R.; Tegeder, P.; Engels, B. Geometry relaxation-mediated localization and delocalization of excitons in organic semiconductors: A quantum chemical study. *J. Chem. Phys.* **2020**, *153*, 224104.
- (20) Meier, T.; Zhao, Y.; Chernyak, V.; Mukamel, S. Polarons, localization, and excitonic coherence in superradiance of biological antenna complexes. *J. Chem. Phys.* **1997**, *107*, 3876–3893.
- (21) Scholes, G. D.; Fleming, G. R.; Chen, L. X.; Aspuru-Guzik, A.; Buchleitner, A.; Coker, D. F.; Engel, G. S.; Van Grondelle, R.; Ishizaki, A.; Jonas, D. M.; et al. Using coherence to enhance function in chemical and biophysical systems. *Nature* **2017**, *543*, 647–656.
- (22) Hecht, M.; Würthner, F. Supramolecularly engineered J-aggregates based on perylene bisimide dyes. *Acc. Chem. Res.* **2021**, *54*, 642–653.
- (23) Würthner, F.; Kaiser, T. E.; Saha-Möller, C. R. J-aggregates: from serendipitous discovery to supramolecular engineering of functional dye materials. *Angew. Chem., Int. Ed.* **2011**, *50*, 3376–3410.
- (24) Tischler, J. R.; Bradley, M. S.; Bulović, V.; Song, J. H.; Nurmikko, A. Strong coupling in a microcavity LED. *Phys. Rev. Lett.* **2005**, *95*, 036401.
- (25) Walker, B. J.; Dorn, A.; Bulovic, V.; Bawendi, M. G. Color-selective photocurrent enhancement in coupled J-aggregate/nanowires formed in solution. *Nano Lett.* **2011**, *11*, 2655–2659.
- (26) Arias, D. H.; Stone, K. W.; Vlaming, S. M.; Walker, B. J.; Bawendi, M. G.; Silbey, R. J.; Bulovic, V.; Nelson, K. A. Thermally-limited exciton delocalization in superradiant molecular aggregates. *J. Phys. Chem. B* **2013**, *117*, 4553–4559.
- (27) Deshmukh, A. P.; Koppel, D.; Chuang, C.; Cadena, D. M.; Cao, J.; Caram, J. R. Design principles for two-dimensional molecular aggregates using Kasha's model: tunable photophysics in near and short-wave infrared. *J. Phys. Chem. C* **2019**, *123*, 18702–18710.
- (28) Nematiram, T.; Padula, D.; Troisi, A. Bright Frenkel excitons in molecular crystals: a survey. *Chem. Mater.* **2021**, *33*, 3368–3378.

- (29) Chuang, C.; Bennett, D. I.; Caram, J. R.; Aspuru-Guzik, A.; Bawendi, M. G.; Cao, J. Generalized kasha's model: T-dependent spectroscopy reveals short-range structures of 2d excitonic systems. *Chem.* **2019**, *5*, 3135–3150.
- (30) Yamagata, H.; Spano, F. C. Interplay between intrachain and interchain interactions in semiconducting polymer assemblies: The HJ-aggregate model. *J. Chem. Phys.* **2012**, *136*, 184901.
- (31) Spano, F. C.; Yamagata, H. Vibronic coupling in J-aggregates and beyond: a direct means of determining the exciton coherence length from the photoluminescence spectrum. *J. Phys. Chem. B* **2011**, *115*, 5133–5143.
- (32) Tretiak, S.; Mukamel, S. Density matrix analysis and simulation of electronic excitations in conjugated and aggregated molecules. *Chem. Rev.* **2002**, *102*, 3171–3212.
- (33) Yuen-Zhou, J.; Krich, J. J.; Mohseni, M.; Aspuru-Guzik, A. Quantum state and process tomography of energy transfer systems via ultrafast spectroscopy. *Proc. Natl. Acad. Sci. U. S. A.* **2011**, *108*, 17615–17620.
- (34) Moix, J. M.; Zhao, Y.; Cao, J. Equilibrium-reduced density matrix formulation: Influence of noise, disorder, and temperature on localization in excitonic systems. *Phys. Rev. B* **2012**, *85*, 115412.
- (35) Fidler, H.; Knoester, J.; Wiersma, D. A. Superradiant emission and optical dephasing in J-aggregates. *Chem. Phys. Lett.* **1990**, *171*, 529–536.
- (36) Kühn, O.; Sundström, V. Pump–probe spectroscopy of dissipative energy transfer dynamics in photosynthetic antenna complexes: A density matrix approach. *J. Chem. Phys.* **1997**, *107*, 4154–4164.
- (37) Sarovar, M.; Ishizaki, A.; Fleming, G. R.; Whaley, K. B. Quantum entanglement in photosynthetic light-harvesting complexes. *Nat. Phys.* **2010**, *6*, 462–467.
- (38) Scholes, G. D. Limits of exciton delocalization in molecular aggregates. *Faraday Discuss.* **2020**, *221*, 265–280.
- (39) Zwolak, M.; Vidal, G. Mixed-state dynamics in one-dimensional quantum lattice systems: a time-dependent superoperator renormalization algorithm. *Phys. Rev. Lett.* **2004**, *93*, 207205.
- (40) Verstraete, F.; Garcia-Ripoll, J. J.; Cirac, J. I. Matrix product density operators: Simulation of finite-temperature and dissipative systems. *Phys. Rev. Lett.* **2004**, *93*, 207204.
- (41) Ren, J.; Shuai, Z.; Kin-Lic Chan, G. Time-dependent density matrix renormalization group algorithms for nearly exact absorption and fluorescence spectra of molecular aggregates at both zero and finite temperature. *J. Chem. Theory Comput.* **2018**, *14*, 5027–5039.
- (42) Ren, J.; Li, W.; Jiang, T.; Shuai, Z. A general automatic method for optimal construction of matrix product operators using bipartite graph theory. *J. Chem. Phys.* **2020**, *153*, 084118.
- (43) Holstein, T. Studies of polaron motion: Part I. The molecular-crystal model. *Ann. Phys.* **1959**, *8*, 325–342.
- (44) Hestand, N. J.; Spano, F. C. Molecular aggregate photophysics beyond the Kasha model: novel design principles for organic materials. *Acc. Chem. Res.* **2017**, *50*, 341–350.
- (45) Sun, Q.; Ren, J.; Jiang, T.; Peng, Q.; Ou, Q.; Shuai, Z. Intermolecular charge-transfer-induced strong optical emission from herringbone H-Aggregates. *Nano Lett.* **2021**, *21*, 5394–5400.
- (46) Sun, Q.; Jiang, T.; Ou, Q.; Peng, Q.; Shuai, Z. Influence of Intermolecular Packing on Light Emitting Efficiency and Carrier-Mobility of Organic Semiconductors: Theoretical Descriptor for Molecular Design. *Adv. Opt. Mater.* **2023**, *11*, 2202621.
- (47) Li, W.; Ren, J.; Shuai, Z. A general charge transport picture for organic semiconductors with nonlocal electron-phonon couplings. *Nat. Commun.* **2021**, *12*, 4260.
- (48) Aragón, J.; Troisi, A. Dynamics of the excitonic coupling in organic crystals. *Phys. Rev. Lett.* **2015**, *114*, 026402.
- (49) Haegeman, J.; Lubich, C.; Oseledets, I.; Vandereycken, B.; Verstraete, F. Unifying time evolution and optimization with matrix product states. *Phys. Rev. B* **2016**, *94*, 165116.
- (50) Würthner, F.; Saha-Moller, C. R.; Fimmel, B.; Ogi, S.; Leowanawat, P.; Schmidt, D. Perylene bisimide dye assemblies as archetype functional supramolecular materials. *Chem. Rev.* **2016**, *116*, 962–1052.
- (51) Gsänger, M.; Bialas, D.; Huang, L.; Stolte, M.; Würthner, F. Organic semiconductors based on dyes and color pigments. *Adv. Mater.* **2016**, *28*, 3615–3645.
- (52) Knapp, E. Lineshapes of molecular aggregates, exchange narrowing and intersite correlation. *Chem. Phys.* **1984**, *85*, 73–82.
- (53) Spano, F.; Silvestri, L. Multiple mode exciton-vibrational coupling in H-aggregates: synergistic enhancement of the quantum yield. *J. Chem. Phys.* **2010**, *132*, 094704.
- (54) Sifain, A. E.; Fassioli, F.; Scholes, G. D. Toward witnessing molecular exciton entanglement from spectroscopy. *Phys. Rev. A* **2021**, *104*, 042416.
- (55) Spano, F. C. Temperature dependent exciton emission from herringbone aggregates of conjugated oligomers. *J. Chem. Phys.* **2004**, *120*, 7643–7658.